

Electronic Supplementary Information

Correlating Hysteresis Phenomena to Interfacial Charge Accumulation in Perovskite Solar Cells

Tianyang Chen, Zhe Sun,* Mao Liang and Song Xue*

Tianjin Key Laboratory of Organic Solar Cells and Photochemical Conversion, School of Chemistry & Chemical Engineering, Tianjin University of Technology, Tianjin 300384, P. R. China.

Fax: +86-22-60214252

Tel: +86-22-60214250

E-mail: zhesun@tjut.edu.cn, xuesong@ustc.edu.cn;

List of Contents

1. Physical model and numerical details.	S1
2. Effect of charge transfer rate constant on photovoltaic performance of PSCs	S8
3. Expression of open circuit voltage	S9
4. Energy diagram of an operating PSC at short and open circuit	S10
5. Profiles of electrostatic voltage and the screening of electric field	S11

1. Physical model and numerical details

Planar perovskite solar cell (PSC), as indicated in Figure S1, is configured as electron selective layer(ESL)|perovskite(PS)|hole selective layer(HSL). The transport of photo-generated electrons and holes throughout PSC is described by drift-diffusion (D-D) equations in 1 D. Current densities of electron (j_n) and hole (j_p) are given by

$$j_n = -\mu_n \left(qn \frac{\partial V}{\partial x} - k_B T \frac{\partial n}{\partial x} \right) \quad (S1)$$

$$j_p = -\mu_p \left(qp \frac{\partial V}{\partial x} + k_B T \frac{\partial p}{\partial x} \right) \quad (S2)$$

where q is the elementary charge, k_B is Boltzmann constant, T is absolute temperature, V is the profile of electrostatic potential, n and p are electron and hole densities, μ_n and μ_p represent the mobility of electron and hole, respectively.

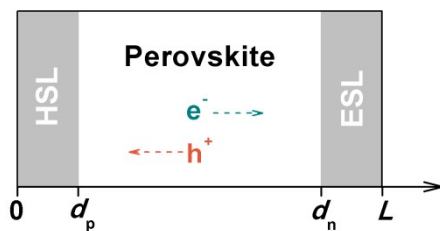


Fig. S1 Schematic of perovskite device. Symbols “ESL” and “HSL” stand for electron selective layer and hole selective layer, respectively. Cartesian coordinates of PS/ESL and HSL/PS interfaces are marked as “ d_n ” and “ d_p ”, respectively.

Movable cations and anions are assumed to redistribute in perovskite layer in response to the variation of electric field. Thereby, current densities of the ions are written as

$$j_a = -\mu_a \left(qa \frac{\partial V}{\partial x} - k_B T \frac{\partial a}{\partial x} \right) \quad (S3)$$

$$j_c = -\mu_c \left(qc \frac{\partial V}{\partial x} + k_B T \frac{\partial c}{\partial x} \right) \quad (S4)$$

where a and c are anion and cation densities, μ_a and μ_c account for the motilities of anion and cation, respectively.

The profile of electrostatic potential is obtained by solving Poisson's equation, which takes the form,

$$\frac{\partial^2 V}{\partial x^2} = \begin{cases} -\frac{q}{\epsilon_0 \epsilon_E} (N_A^- - p) & x \in [0, d_p) \\ -\frac{q}{\epsilon_0 \epsilon_{PS}} (n - p + a - c) & x \in [d_p, d_n] \\ -\frac{q}{\epsilon_0 \epsilon_H} (n - N_D^+) & x \in (d_n, L] \end{cases} \quad (S5)$$

where ϵ_0 is vacuum permittivity, ϵ_E , ϵ_{PS} , and ϵ_H are relative permittivity for SEL, perovskite layer, and HSL, respectively. Parameters N_A^- and N_D^+ indicate the densities of ionized n-type and p-type dopants in hole and electron selective layers, respectively.

When PSC is operating in steady state, the distributions of electron, hole, anion, and cation obey the continuity equations,

$$\begin{cases} \frac{\partial j_p}{\partial x} = 0 & x \in [0, d_p) \\ \frac{1}{q} \frac{\partial j_T}{\partial x} = \nu (G_{in} - R_r) & x \in [d_p, d_n] \\ \frac{\partial j_n}{\partial x} = 0 & x \in (d_n, L] \end{cases} \quad (S6)$$

where subscript "T" stands for n, p, a, and c. The prefactor ν is given by

$$v = \begin{cases} 1 & T = p \\ -1 & T = n \\ 0 & T = a \text{ or } c \end{cases} \quad (S7)$$

The rate of electron/hole generation G_{in} is assumed to be invariant. Charge loss is attributed to bulk recombination inside perovskite layer and surface recombination at the contacts between perovskite and charge selective layers. Bulk recombination is described by using bimolecular model. Accordingly, recombination rate is written as

$$R_b = k_{rb}(np - n_i^2) \quad (S8)$$

Where k_{rb} is bimolecular recombination rate constant, n_i is intrinsic carrier density. In addition, surface recombination is assumed to occur via trapping states. It follows that surface recombination rate is evaluated based on Shockley–Read–Hall (SRH) equation, ¹

$$R_{SRH} = \frac{np - n_i^2}{(n + n_1)/k_{sp} + (p + p_1)/k_{sn}} \quad (S9)$$

where n_1 and p_1 are the densities of electron and hole at trapping state, k_{sp} and k_{sn} are the rate constant. According to the model by Courtier et al., surface recombination at ESL/PS boundary is limited by the density of trapped electrons and free holes in PS surface, while the recombination at PS/HSL boundary is determined by the density of trapped holes and free electrons.²⁻³ Eqn S9 is reduced to

$$R_{SRH}|_{d_p} = k_{sp}p \quad (S10)$$

$$R_{SRH}|_{d_n} = k_{sn}n \quad (S11)$$

Note that k_{sp} and k_{sn} are assumed to be equal. They are both termed as k_s in our simulations for simplicity.

Boundary conditions for solving drift-diffusion equations s5 and s6 are summarized as follows:

$$\begin{aligned}
 p(0) &= p_0 \\
 n(L) &= n_0 \\
 j_n(d_p) &= 0 \\
 j_p(d_n) &= 0 \\
 V(0) &= V_{app} - V_{bi}/2 \\
 V(L) &= \frac{V_{bi}}{2}
 \end{aligned}$$

where V_{app} is the bias voltage applied to the metallic contacts of PSCs, V_{bi} is built-in electric field.

The electric displacement at the ESL/PS and PS/HSL interfaces is formulated by

$$\epsilon_{PS}\nabla_x V(d_n)|_+ = \epsilon_E\nabla_x V(d_n)|_- \quad (S18)$$

$$\epsilon_H\nabla_x V(d_p)|_+ = \epsilon_{PS}\nabla_x V(d_p)|_- \quad (S19)$$

Charge transfer crossing ESL/PS and PS/HSL interfaces is assumed to be driven by the difference of the Fermi-level at two sides of each contact. Assuming equal exchange rate constant (k_{et}) for the forward and reverse charge transfer direction, charge transfer current (j_{tr}) is given by,

$$j_{tr}^n = qk_{et}[\exp(-\alpha\eta_n) - \exp(\alpha(1-\alpha)\eta_n)] \quad (S20)$$

$$j_{tr}^p = qk_{et}[\exp(-\alpha\eta_p) - \exp(\alpha(1-\alpha)\eta_p)] \quad (S21)$$

where α is charge transfer coefficient, and η_n and η_p are the Fermi-level difference at ESL/PS and PS/HSL boundaries, respectively. The η_n and η_p are given by,

$$\eta_n = E_{F,n}(d_n^-) - E_{F,n}(d_n^+) \quad (S22)$$

$$\eta_p = E_{F,n}(d_p^+) - E_{F,n}(d_p^-) \quad (S23)$$

where subscripts “-” and “+” indicate the right and left side of the interface, respectively.

The operation of DSCs is mimicked by solving the D-D equations (eqns S5 and S6) numerically. Kinetics of charge extraction at HSL/PS and PS/ESL contacts is considered by incorporating eqns S20 and S21 into the equation set. The resultant equation system was solved by using finite-difference scheme in conjunction with relaxed iterative algorithm. Parameters utilized for simulation are enlisted in Table S1. Spatial variables, such as n , p , a , c , and V , are discretized with non-uniform grid meshing. As indicated in Figure S2, fine-meshing of 0.1 nm is applied to the domains of 20 nm centering at the PS/ESL and HSL/PS boundaries. Those red domains are demonstrated to be wide enough to cover the narrow Debye layer, and hence give rise to a good convergence. In the rest of the domains, coarse-grained grid of 5 nm is employed for balancing computation time and the precision of solution.

When simulating j - V hysteresis, model device is firstly preconditioned at the bias voltage of 0 and 1.2 V for forward and reverse scans, respectively. In this scenario, both charge carriers and movable ions are allowed to relax to their equilibrium profiles. After the preconditioning, swift j - V scanning is performed in which the distribution of electron and hole evolve at each scan step while mobile ions are frozen at their initial position.

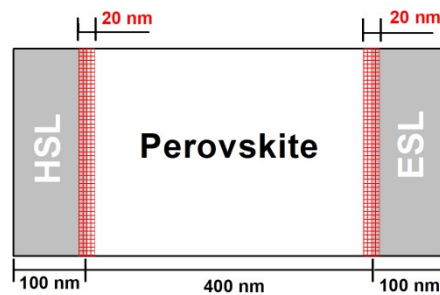


Fig. S2 Schematic of spatial meshing in perovskite device. Red girds highlight the parts where fine-grid meshing is employed in simulation.

Table S1 Parameters for Device Simulation.

Parameter	Symbol	Unit	Value	References
Conduction band edge in perovskite	E_c^{PS}	eV	-3.93	4
Valence band edge in perovskite	E_v^{PS}	eV	-5.43	4
Conduction band edge in ESL	E_c^E	eV	-4.0	5
Valence band edge in HSL	E_v^H	eV	-5.22	6
relative permittivity of perovskite	ϵ_{PS}	–	6.5	7
Relative permittivity of ESL	ϵ_E	–	80.0	
Relative permittivity of HSL	ϵ_H	–	3.0	7
Electron mobility in perovskite	μ_n^{PS}	$cm^2 V^{-1} s^{-1}$	9.90	8
Hole mobility in perovskite	μ_p^{PS}	$cm^2 V^{-1} s^{-1}$	9.90	7
Electron mobility in ESL	μ_n^E	$cm^2 V^{-1} s^{-1}$	4.0×10^{-5}	9
Hole mobility in HSL	μ_p^H	$cm^2 V^{-1} s^{-1}$	1×10^{-3}	9
Charge generation rate	G_{in}	$cm^{-3} s^{-1}$	3.4×10^{21}	10
Bimolecular recombination rate constant	k_{rb}	$cm^3 s^{-1}$	6×10^{-8} 6×10^{-12}	
Exchange rate constant	k_s	$cm^{-2} s^{-1}$	0.01~0.1	
Charge transfer coefficient,	α	–	0.5	11
Density of states (DOS)	N_0	cm^{-3}	6×10^{19}	
Mobile cation concentration	N_{ca}	cm^{-3}	1×10^{18}	12
Mobile anion concentration	N_{an}	cm^{-3}	1×10^{18}	12

Acceptor concentration	N_A^-	cm^{-3}	5×10^{17}	13
Donor concentration	N_D^+	cm^{-3}	5×10^{17}	13
Position of HSL/PS contact	d_p	nm	100	
Position of PS/ESL contact	d_n	nm	500	
Thickness of device	L	nm	600	
Sparse grid size	Δx_S	nm	5	
Fine grid size	Δx_F	nm	0.1	

2. Effect of charge transfer rate constant on photovoltaic performance of PSCs

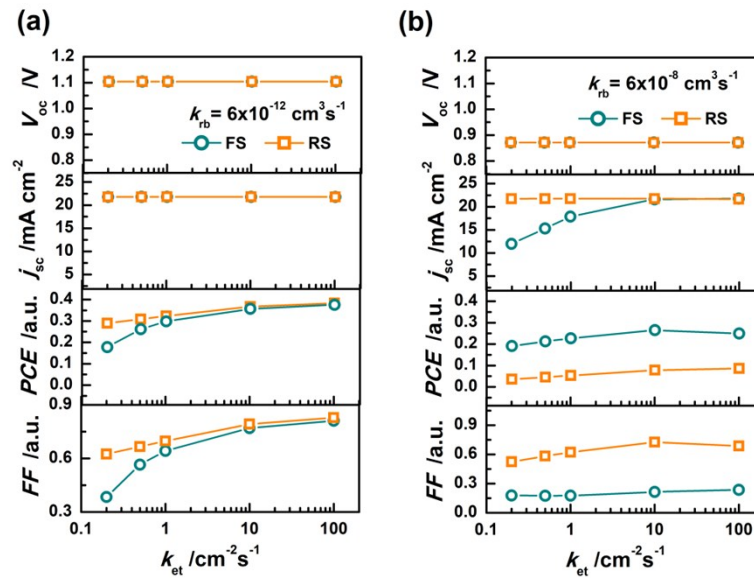


Fig. S3 Photovoltaic parameters for PSCs with variable charge transfer rate constant. Green and yellow curves are obtained under forward and reverse scans, respectively. In images a and b, recombination

rate constant k_{rb} equals to 6×10^{-12} and $6 \times 10^{-8} \text{ cm}^3\text{s}^{-1}$, respectively. V_{oc} : open circuit voltage, j_{sc} : short circuit current density, η : energy conversion efficiency, FF : fill factor.

3. Expression of open circuit voltage

When an irradiated PSC is measured at open circuit, photogenerated electrons and holes are recombined entirely in device, namely light harvesting flux equals to recombination rate. The recombination rate is evaluated herein by considering the contributions of both radiative recombination in the bulk and surface recombination. By using eqns S8 and S9, the relationship is formulated by

$$I_0 \eta_{LH} = \int_{d_p}^{d_n} \left(k_{rb} (np - n_i^2) + \frac{np - n_i^2}{(n + n_1)/k_{sp} + (p + p_1)/k_{sn}} \delta_{surf} \right) dx \quad (S24)$$

where δ_{surf} is the Dirac symbol which ensures the trap-mediated recombination occurs at the PS/ESL and HSL/PS contacts.

As demonstrated in Figure S3, the Fermi-level of either electron or hole is invariant to coordinate. The product of n and p is thereby related to the difference between open circuit voltage and the band gap, which is given by

$$np = N_0^2 \exp\left(\frac{q}{k_B T} (V_{oc} - E_g)\right) \quad (S25)$$

where V_{oc} is open circuit voltage, which is defined as the difference of the quasi-Fermi level between electron and hole, N_0 is the density of state. After the insertion of eqn S23 into eqn S22, V_{oc} is expressed as

$$V_{oc} = E_g + \frac{k_B T}{q} \ln \left(\frac{I_0 \eta_{LH}}{N_0^2} \left(k_{rb} + \sum_{x=d_n, d_p} \frac{w_L}{(n+n_1)/k_{sp} + (p+p_1)/k_{sn}} \right)^{-1} \right) \quad (S26)$$

where w_L is the width of the domain that the traps are localized adjacent to the interfaces.

If surface recombination is neglected, one will find V_{oc} is independent of the density profiles of electron and hole, not to mention the electric field. Thereby, the j - V curves under forward and reverse scans will meet at the point of V_{oc} once charge carriers are only consumed by bulk recombination.

4. Energy diagram of an operating PSC at short and open circuit

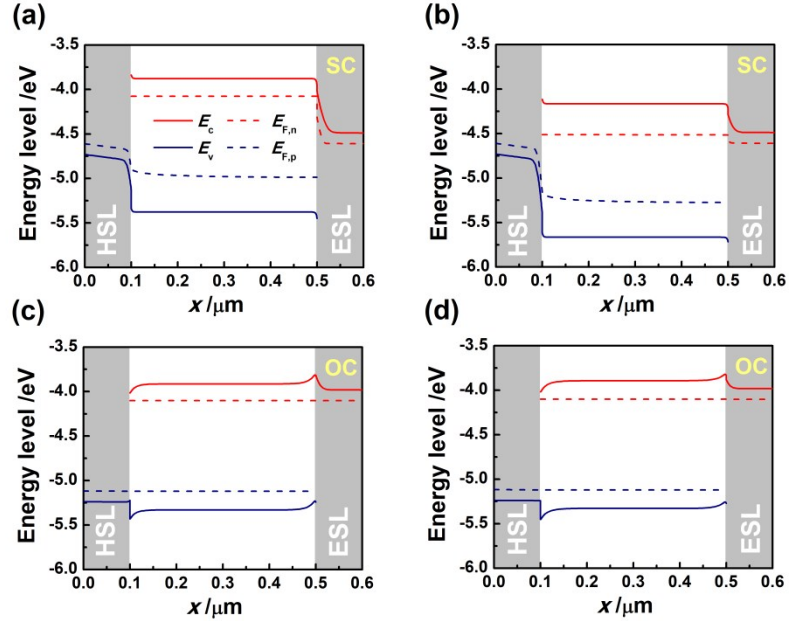


Fig. S4 Energy diagram of the PSC at short circuit (a, b) and open circuit (c, d). Charge transfer rate constant in images (a, c) and (b, d) is 0.2 and 10 $\text{cm}^{-2} \text{s}^{-1}$, respectively. Recombination rate constant k_{rb} is $6 \times 10^{-12} \text{cm}^3 \text{s}^{-1}$.

5. Profiles of electrostatic voltage and the screening of electric field

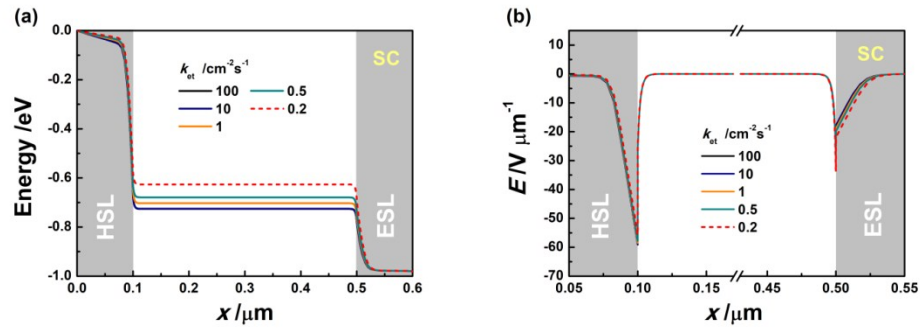


Fig. S5 Profiles of electrostatic voltage (a) and electric field (b) at short circuit. Recombination rate constant k_{rb} is $6 \times 10^{-8} \text{ cm}^2 \text{ s}^{-1}$.

References

1. Shockley, W.; Read, W. T., Statistics of the Recombinations of Holes and Electrons. *Phys. Rev.* **1952**, *87*, 835-842.
2. Courtier, N. E.; Cave, J. M.; Foster, J. M.; Walker, A. B.; Richardson, G., How Transport Layer Properties Affect Perovskite Solar Cell Performance: Insights from a Coupled Charge Transport/Ion Migration Model. *Energy Environ. Sci.* **2019**, *12*, 396-409.
3. Tress, W.; Petrich, A.; Hummert, M.; Hein, M.; Leo, K.; Riede, M., Imbalanced Mobilities Causing S-Shaped Iv Curves in Planar Heterojunction Organic Solar Cells. *Appl. Phys. Lett.* **2011**, *98*, 063301.

4. Etgar, L.; Gao, P.; Xue, Z.; Peng, Q.; Chandiran, A. K.; Liu, B.; Nazeeruddin, M. K.; Gratzel, M., Mesoscopic CH₃NH₃PbI₃/TiO₂ Heterojunction Solar Cells. *J. Am. Chem. Soc.* **2012**, *134*, 17396-9.
5. Xue, H.; Fu, K.; Wong, L. H.; Birgersson, E.; Stangl, R., Modelling and Loss Analysis of Meso-Structured Perovskite Solar Cells. *J. Appl. Phys.* **2017**, *122*, 083105.
6. Do, K.; Choi, H.; Lim, K.; Jo, H.; Cho, J. W.; Nazeeruddin, M. K.; Ko, J., Star-Shaped Hole Transporting Materials with a Triazine Unit for Efficient Perovskite Solar Cells. *Chem. commun.* **2014**, *50*, 10971-4.
7. Foster, J. M.; Snaith, H. J.; Leijtens, T.; Richardson, G., A Model for the Operation of Perovskite Based Hybrid Solar Cells: Formulation, Analysis, and Comparison to Experiment. *SIAM J. Appl. Math.* **2014**, *74*, 1935-1966.
8. Herz, L. M., Charge-Carrier Mobilities in Metal Halide Perovskites: Fundamental Mechanisms and Limits. *ACS Energy Lett.* **2017**, *2*, 1539-1548.
9. Leijtens, T.; Lim, J.; Teuscher, J.; Park, T.; Snaith, H. J., Charge Density Dependent Mobility of Organic Hole-Transporters and Mesoporous TiO₂ Determined by Transient Mobility Spectroscopy: Implications to Dye-Sensitized and Organic Solar Cells. *Adv. Mater.* **2013**, *25*, 3227-33.
10. van Reenen, S.; Kemerink, M.; Snaith, H. J., Modeling Anomalous Hysteresis in Perovskite Solar Cells. *J. Phys. Chem. Lett.* **2015**, *6*, 3808-14.
11. Bai, P.; Bazant, M. Z., Charge Transfer Kinetics at the Solid-Solid Interface in Porous Electrodes. *Nat Commun.* **2014**, *5*, 3585.
12. Neukom, M. T.; Züfle, S.; Knapp, E.; Makha, M.; Hany, R.; Ruhstaller, B., Why Perovskite Solar Cells with High Efficiency Show Small I_v-Curve Hysteresis. *Sol. Energy Mater. Sol. Cells* **2017**, *169*, 159-166.

13. Calado, P.; Telford, A. M.; Bryant, D.; Li, X.; Nelson, J.; O'Regan, B. C.; Barnes, P. R., Evidence for Ion Migration in Hybrid Perovskite Solar Cells with Minimal Hysteresis. *Nat Commun* **2016**, *7*, 13831.